J. Fluid Mech. (2001), *vol.* 430, *pp.* 149–168. Printed in the United Kingdom

Disturbance growth in boundary layers subjected to free-stream turbulence

By M. MATSUBARA† AND P. H. ALFREDSSON

Department of Mechanics, KTH, S-100 44, Stockholm, Sweden

(Received 28 May 1999 and in revised form 5 September 2000)

This paper aims at a description of boundary-layer flow which is subjected to free-stream turbulence in the range from 1–6% and is based on both flow visualization results and extensive hot-wire measurements. Such flows develop streamwise elongated regions of high and low streamwise velocity which seem to lead to secondary instability and breakdown to turbulence. The initial growth of the streaky structures is found to be closely related to algebraic or transient growth theory. The data have been used to determine streamwise and spanwise scales of the streaky structures. Both the flow visualization and the hot-wire measurements show that close to the leading edge the spanwise scale is large as compared to the boundary-layer thickness, but further downstream the spanwise scale approaches the boundary-layer thickness. Wavenumber spectra in both the streamwise and the spanwise directions were calculated. A scaling for the streamwise structure of the disturbance was found, which allows us to collapse the spectra from different downstream positions. The scaling combines the facts that the streaky structures increase their streamwise length in the downstream direction which becomes proportional to the boundary-layer thickness and that the energy growth is algebraic, close to proportional to the downstream distance.

1. Introduction

Transition to turbulence in laminar boundary layers subjected to high levels of free-stream turbulence (FST) can still not be reliably predicted, despite its technical importance, e.g. in the case of boundary layers developing on gas turbine blades. Under these conditions laminar boundary layers may exhibit a rapid breakdown to turbulence, which cannot be explained by the traditional scenario based on the growth of Tollmien–Schlichting (TS) waves, and is therefore usually denoted as bypass transition. At present, there does not exist any reliable method for transition prediction at high levels of FST (see e.g. Westin & Henkes 1997) and is a serious problem in the design process for certain applications. For instance the chord Reynolds number on a turbine blade in a low pressure turbine is relatively small (of the order of 10^5), and therefore a significant part of the blade experiences laminar and/or transitional flow.

1.1. *Previous experimental work*

There has recently been several experimental studies with the aim to study boundary layers under the influence of FST. Recent reviews are given by Kendall (1998) and in the doctoral thesis of Westin (1997). We do not intend here to give a full review of

† Present address: Department of Mechanical Systems Engineering, Shinshu University, Nagano, Japan.

earlier studies, but will outline the present picture of the boundary-layer development, with references to the relevant literature.

It is known from both flow visualization and hot-wire measurements that a boundary layer subjected to FST develops unsteady streaky structures with high and low streamwise velocity. The first reference to such disturbances is usually ascribed to Klebanoff (1971), although already Dryden (1937) and Taylor (1939) reported some experimental reults about boundary-layer disturbances which were associated with FST. Also, Arnal & Juillen (1978) showed that at high levels of FST, i.e. higher than about 0.5–1%, the dominant disturbances in the boundary layer are not TS-waves. The energy of the dominant disturbances is found at rather low frequencies and the maximum of the streamwise velocity disturbance is approximately located in the middle of the boundary layer. They found that the amplitude of u_{rms} is in the range 5–7% of the free-stream velocity (U_∞) before transition starts. As comparison, a TS-wave has its maximum amplitude much closer to the wall and TS-waves break down at amplitudes of the order of 1%.

Kendall (1985) observed elongated streamwise structures with narrow spanwise scales in a laminar boundary layer subjected to FST and he denoted these disturbances Klebanoff modes. He found that the maximum disturbance level in the boundary layer grows in linear proportion to $x^{1/2}$ (i.e. proportional to the laminar boundary-layer thickness). Also, Westin *et al.* (1994) made detailed measurements of a laminar boundary layer disturbed by FST and showed among other things that the Blasius profile is only slightly modified, despite u_{rms} levels of about 10% inside the boundary layer before breakdown. Their data confirmed that u_{rms} increases as $x^{1/2}$ and they also compiled data from other studies and showed that this was a general observation. However, they showed that the growth rate as well as the level of u_{rms} where transition occurs vary considerably between different studies.

A hypothesis is that breakdown to turbulence is caused through a secondary instability developing on the streaks which leads to the formation of turbulent spots. A study by Westin *et al.* (1998), where a single streaky structure was modelled through a localized free-stream disturbance, showed that the disturbance increases in length but decreases in amplitude as it propagates downstream in the boundary layer. A possible triggering mechanism for the secondary instability could be Tollmien–Schlichting waves that may coexist with the streaky structures. Such studies have been made by Boiko *et al.* (1994), Grek, Kozlov & Ramazanov (1990) and Kosorygin & Polyakov (1990). In the study of Boiko *et al.* (1994) it was found that the introduction of TS-waves enhances the breakdown to turbulence. In a follow-up experiment to that of Westin *et al.* (1998), Bakchinov *et al.* (1998) showed that even damped TS-waves which are introduced together with a streaky structure develop strong nonlinearities which lead to breakdown of the streaky structure and the formation of an incipient spot. However, there may also be other sources behind the triggering of secondary instabilities, such as the continuous forcing by the free-stream turbulence, which can be viewed as a distributed small-scale disturbance, not necessarily giving rise to TS-waves. Other experiments where the location and extent of the transitional region were documented are the studies of Suder, O'Brien & Reshotko (1988) and Roach & Brierly (1992).

The above description of the various stages in the transition process shows that accurate physical modelling of several aspects is probably required to obtain a reliable prediction method for transition in boundary layers subjected to FST. These processes include the formation and growth of streaky structures, the development of secondary instabilities, the formation of the incipient spot as well as the growth and merger of turbulent spots.

1.2. *Non-modal disturbance growth*

Ellingsen & Palm (1975) and Landahl (1980), proposed that three-dimensional disturbances can grow algebraically in shear flows, a scenario which differs from the traditional exponentially growing TS-wave disturbance. Landahl used the inviscid normal vorticity equation to show that a disturbance in the normal vorticity may grow linearly (algebraically) in time to infinite amplitude, if forced by the normal velocity. This theory was later extended by Gustavsson (1991) to the viscous case. In that case, viscosity will set a limit on the maximum growth, i.e. the disturbance will ultimately decay. It is interesting to note, however, that a growth may occur also for Reynolds numbers for which modal disturbances (i.e. TS-waves) would decay. He also showed that, in channel flow, the growth rate scales with the Reynolds number, i.e. the time to reach a certain growth is proportional to R^{-1} ($R = U_{CL}h/\nu$, where U_{CL} is the laminar centreline velocity, h is half the channel height and ν is the kinematic viscosity). For infinitely long disturbances, Gustavsson found that the largest amplification occurred for spanwise wavenumbers close to $\beta = 2$ ($\beta = 2\pi h/\lambda$, where λ is the spanwise wavelength), although the wavenumber dependence was not very strong. Butler & Farrell (1992) extended this work by determining the optimal perturbations for plane Poiseuille and Couette flow as well as a (parallel) Blasius boundary-layer flow.

A drawback of the early studies is that they treat the temporal problem, i.e. how a disturbance will grow in time. In a boundary layer, the appropriate viewpoint would be to study disturbances that grow in space. It should be noted that in spatially growing boundary-layer flows it is not necessarily true that algebraic growth will be followed by viscous decay. On the contrary, Luchini (1996) showed the existence of three-dimensional self-similar solutions where the streamwise disturbance velocity grows as $x^{0.213}$. (The coordinate system used in this paper is x for the streamwise direction, where $x = 0$ is at the plate leading edge, y is the coordinate normal to the plate with $y = 0$ at the plate, and z is the spanwise coordinate.) He also predicted disturbance profiles of the streamwise velocity which are in excellent agreement with recent measurements. This indicates that non-modal growth may be important for boundary-layer transition in the case of excitation by three-dimensional disturbances (such as localized roughness elements or free-stream turbulence).

Luchini (2000) showed that if optimal perturbations are used, i.e. perturbations that maximize the energy growth, the energy growth is actually proportional to x (or equivalently the streamwise disturbance velocity increases as $x^{0.5}$). In his analysis the disturbance with the largest growth at a given x is obtained when $\beta\delta^* = 0.77$ (δ^* is the displacement thickness of the boundary layer). This means that the spanwise size of the optimal disturbance is approximately 40% larger than the boundary-layer thickness at a given downstream position and that the optimal spanwise scale increases as $x^{0.5}$ in the downstream direction.

Andersson, Berggren & Henningson (1999) worked along similar lines to Luchini (2000) and found the same optimal spanwise scale. They showed that a fixed spanwise wavenumber in terms of physical units also can give a similar, nearly linear initial growth of the disturbance energy as well as disturbance profiles which are in good agreement with measured r.m.s.-profiles in a boundary layer subjected to free-stream turbulence. Furthermore, they argue that the Reynolds number for transition onset is inversely proportional to the square of the FST intensity and they were able to correlate data from several studies with this hypothesis. It should be pointed out (e.g. see Waleffe 1997) that transient growth of streaky structures is only the first step towards transition, the latter stages must involve nonlinear effects. The model of Andersson *et al.* does not take into account any of the nonlinear processes which must

be active before transition occurs, but is, on the other hand, successful in correlating available data.

In the studies discussed so far, the receptivity mechanism of the boundary layer has not been an issue, rather the studies have started when the disturbance has been assumed to be inside the boundary layer already. Bertolotti (1997) studied the effect of vortical modes in the free-stream on the development of disturbances in a Blasius boundary layer using the parabolized stability equations (PSE). Low-frequency and stationary modes were found to give disturbances in the boundary layer that are in good agreement with experiments.

A different type of analysis is that of Goldstein and co-workers (see for instance Goldstein & Wundrow 1998; Leib, Wundrow & Goldstein 1999), where the linear boundary-region equations are solved assuming a certain free-stream disturbance spectrum. Their calculations indicate that it is the low-frequency content of the fluctuating transverse velocity components in the FST that actually triggers the Klebanoff modes in the boundary layer, and that this is through a linear mechanism. Their solution to the linear equations shows an initial growth of the streamwise disturbance inside the boundary layer which is proportional to $x^{1/2}$ and the disturbance has its maximum in the centre of the boundary layer. Leib *et al.* were able to find good quantitative agreement with the disturbance growth and amplitudes in several experimental studies through this procedure.

1.3. *Streaky structures, oblique transition and transient growth*

Although several experimental studies have dealt with FST directly, some studies of idealized geometries or disturbance sources may also be of interest in order to elucidate the mechanisms behind the FST-induced transition. In particular, the so-called oblique transition concept, which was introduced by Schmid & Henningson (1992), gives some further insights into the processes. The starting point is the introduction of two oblique waves of small but finite amplitude. The wave-pair can be characterized by $(\omega, \pm\beta)$, where ω is their angular frequency and $\pm\beta$ their spanwise wavenumbers. They may interact nonlinearly, and formally it can be stated that the first generation interaction will give components characterized by $(0,0)$, $(2\omega,0)$, $(2\omega,\pm2\beta)$ and $(0,\pm2\beta)$, where the fourth corresponds to a stationary, spanwise periodic disturbance. It was found by Schmid & Henningson (1992) that initially the $(0,\pm2\beta)$ mode reaches high amplitudes through transient growth. The result is a streaky structure in the streamwise velocity. Elofsson & Alfredsson (1998) verified experimentally the existence of the streaky structures in measurements on the interaction between a pair of oblique waves in plane Poiseuille flow.

The oblique transition scenario consists of the following three stages: first, nonlinear generation of streamwise vortices by a pair of oblique waves giving rise to streaks, secondly, transient growth of streaks, and thirdly, breakdown of the flow owing to a secondary instability of the streaks provided their amplitude exceeds a threshold amplitude. It seems probable that FST-induced transition includes the two latter phases in this scenario; however, the intial creation of the streamwise oriented structures is different. The secondary-instability phase has recently been investigated theoretically/numerically by Reddy *et al.* (1998) and by Elofsson, Kawakami & Alfredsson (1999) in plane channel flows. The results of Reddy *et al.*, obtained from both direct numerical simulations and stability calculations, indicate that the secondary instability is due mainly to spanwise inflectional profiles associated with the streaky structures. These findings were corroborated by the experiments by Elofsson *et al.* who also showed that the most amplified secondary wave has a streamwise wavenumber close to the spanwise wavenumber of the streaky structure. They concluded that transition originates from this secondary instability.

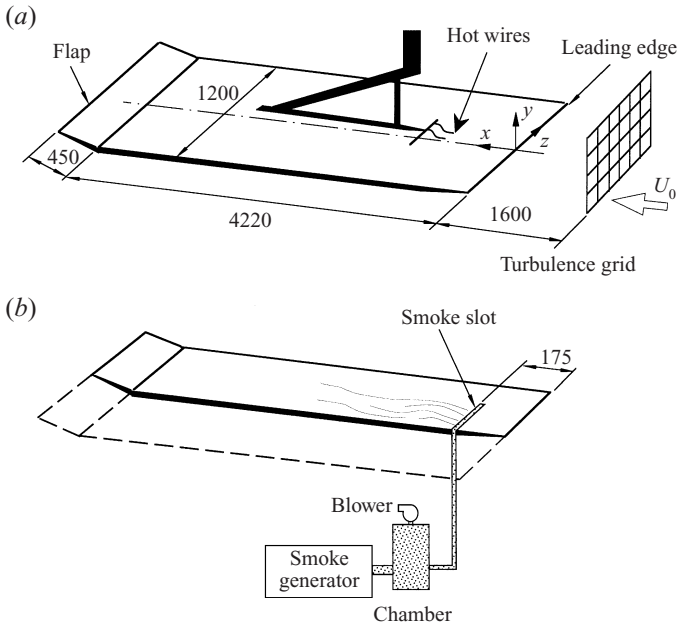

FIGURE 1. Experimental set-up. (*a*) Set-up for hot-wire measurements; (*b*) set-up for flow visualization.

1.4. *Motivation of present work*

The present investigation uses flow visualization and hot-wire anemometry to describe the FST-induced disturbances inside a boundary layer both qualitatively and quantitatively. It also makes extensive comparisons with theoretical work dealing with non-modal growth, as well as other experiments which have studied FST dominated transition or other types of transition where transiently growing disturbances is the first step towards transition. In § 2 we describe the experimental set-up and measurement techniques, i.e. the wind tunnel, turbulence grids, flat plate, as well as the hot-wire and flow visualization set-ups, and finally the data evaluation procedures. Section 3 contains some basic results of the boundary-layer flow, such as velocity data (mean velocity and r.m.s. distributions), integral boundary parameters, etc. as well as some data showing the intermittency as a measure of the stage of transition. The main part of the present work is contained in § 4 where both flow-visualization and hot-wire data are presented, analysed and compared. Various types of scaling of the results are carried out. The results are discussed in § 5 together with comparisons with other investigations.

2. Experimental description

2.1. *Set-up*

The experiments were made in the MTL wind tunnel at KTH, Stockholm. A diagram of the experimental set-up is given in figure 1. The test section is 1.2 m wide, 0.8 m high and 7 m long, and the horizontal test plate spans the whole width of the test section. The test plate is mounted on two rails which run along the test-section floor and these position the test surface approximately 60 cm from the test-section ceiling. The test-plate leading edge is located 1.6 m from the start of the test section and

Grid	Tu (%)	M (mm)	d (mm)	Bar geometry	x_{grid} (m)
A	2.2	36	6	round	−1.6
B	1.5	23	3.5	round	−1.6
E	6.6	50	10	square	−1.0

TABLE 1. Characteristics of the grids used. M is the mesh width, d the bar diameter and Tu the turbulence level at $x = 0$.

the working length of the plate is 2.16 m. An extra plate section of 2 m was added downstream of the test plate and was followed by a trailing-edge flap. The extra plate section was installed in order to minimize the influence of the trailing-edge flap on the boundary layer at the end of the test plate. The trailing-edge flap made it possible to position the stagnation line at the leading edge, on the upper side of the plate to avoid separation. The asymmetric leading edge of the flat plate was specially designed for this set-up to minimize the pressure gradient on the plate upper side. Further details of the plate can be found in Westin *et al.* (1994).

The free-stream turbulence was generated by grids of various sizes mounted in front of the plate in the test section. In the present study, three different grids were used and the data of the grids are given in table 1. The distance from the grid to the plate leading edge was 1.6 m (grids A and B) or 1.0 m (grid E). The development length for the grid-generated turbulence was, in all cases, larger than 20 mesh widths, which is sufficient to obtain a fairly homogeneous turbulence structure. The turbulence level at the plate leading edge was in the range 1.5–6.6% depending on the grid used. For all grids, the Taylor scale for the transverse velocity component of the FST was 5 mm ($\pm$1 mm) at $U_\infty = 8\,\mathrm{m\,s^{-1}}$ as determined from both autocorrelation and two-probe correlation hot-wire (X-probe) measurements.

2.2. *Measurement techniques*

Flow visualization was carried out by letting smoke seep slowly through a spanwise slot (1 mm wide in the streamwise direction and 400 mm long in the spanwise direction). The slot was located 175 mm from the leading edge of the flat plate. In the absence of grids in the tunnel, the smoke formed a homogeneous layer very close to the black-painted surface. Both video and photographic recordings of the flow structures were made. The cameras were mounted at the top of the test section, and optical access was obtained through a hole at the centreline of the ceiling. The light source for the still photographs was an ordinary flashlight mounted at one of the sidewalls inside the wind tunnel, approximately 3 m downstream of the plate leading edge. The light source for the video recordings was a 1000 W floodlight which was also mounted inside the wind tunnel.

The velocity measurements were made with hot-wire anemometry, and for details of calibration procedures and measurement accuracy see Westin *et al.* (1994). In the present experiments, the free-stream velocity was in the range up to $12\,\mathrm{m\,s^{-1}}$. The wind tunnel is equipped with a traversing system which in the present set-up allows movements along the test section and normal to the plate. At the end of the sting a small traverse is mounted which allows one probe to be moved in the spanwise direction, whereas another probe is fixed to the sting. The movement with this traverse is limited to 150 mm, but, in the present study, the maximum spanwise separation of the probes was 60 mm. It is important that the two probes are located at the same y-position and it was checked by comparing the mean velocity measured by the two

probes inside the boundary-layer. For all measurements, the variation of the mean velocity between the probes was within $\pm 5\%$.

2.3. *Data evaluation procedure*

Both hot-wire data and flow-visualization sequences were used to evaluate the spanwise scales of the structures within the boundary layer.

Video sequences of the smoke visualization could be analysed by recording a line in the picture, i.e. a line at a fixed x, over a long period of time. In this way, a picture of the smoke pattern at this x-position is given as a function of time and a spanwise correlation can be determined from the picture.

Two types of spectra were evaluated from the hot-wire data, namely, streamwise wavenumber spectra which were obtained from the frequency spectra measured by the hot-wire at a fixed x-position and converted to wavenumber using the free-stream velocity and spanwise wavenumber spectra which were calculated from data taken simultaneously with two hot wires separated in the spanwise direction.

The streamwise wavenumber spectra were calculated from the energy density spectra obtained from a fast Fourier transform-analysis of the hot-wire signal $e_f(f)$, where the frequency was converted to a wavenumber through

$$\alpha = \frac{2\pi f}{U_\infty}.$$

We then make the wavenumber non-dimensional with the local displacement thickness obtained from the Blasius solution, i.e. $\delta^* = 1.72\sqrt{\nu x/U_\infty}$ giving $\alpha^* = \alpha\delta^*$. This will give us the wavenumber spectral density as

$$E_\alpha(\alpha^*) = \frac{U_\infty}{2\pi\delta^*} e_f.$$

In order to compare spectra obtained at different free-stream velocities, we will first normalize the spectral energy with U_∞^2. In order to take into account the growth of the disturbance energy in the x-direction (as will be shown in § 3, the energy grows linearly with x), we assume that the growth in energy is proportional to Re_x, which is also in accordance with the theoretical argument presented in § 1. Finally, our normalized spectral density can be written as

$$E_\alpha^* = \frac{E_\alpha}{U_\infty^2 Re_x}.$$

The spanwise wavenumber spectra were obtained from a Fourier transformation of the spanwise correlation function, using an interpolation scheme to have constant spacing between grid points. Typically, the spanwise correlation function was determined at 45 different spacings.

3. Basic flow data

This section gives an overview of mean flow data which will be useful to have as a background when studying the flow structures of the transitional boundary layer. We show data only for one case, but the boundary-layer development is similar for all cases studied.

Figure 2 gives an overview of the boundary-layer development. Figure 2(*a*) shows the mean velocity profiles starting at $x = 100$ mm with intervals of 200 mm up to 1900 mm for the case of Grid B and with a free-stream velocity of $U_\infty = 12\,\mathrm{m\,s^{-1}}$.

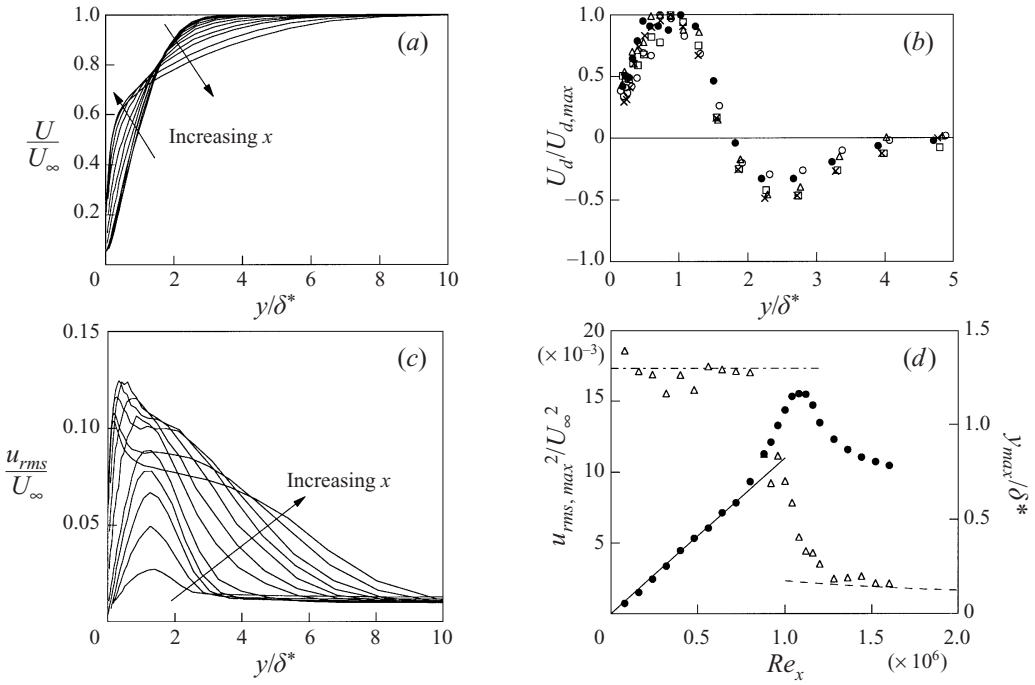

FIGURE 2. Hot-wire measurements at different downstream positions of the streamwise velocity component inside the boundary layer. Grid B. $U_\infty = 12\,\mathrm{m\,s^{-1}}$. (*a*) Mean velocity ($U$), $x = 100, 300, 500, \ldots, 1900\,\mathrm{mm}$. (*b*) Deviation of the mean velocity from the Blasius solution, normalised with its maximum value, ○, $x = 700\,\mathrm{mm}$; △, $x = 800\,\mathrm{mm}$; □, $x = 900\,\mathrm{mm}$; ×, $x = 1000\,\mathrm{mm}$; ●, $x = 1100\,\mathrm{mm}$. (*c*) u_{rms}-Distributions for the same x-positions as in (*a*). (*d*) ●, maximum of u_{rms}^2; △, position of maximum of u_{rms} as function of Re_x; $-\cdot-$, $y/\delta^* = 1.30$; $---$, $y^+ \approx 15$.

The boundary-layer behaviour was illustrated with such a high free-stream velocity because for this case, the boundary layer goes through all its main stages, namely the non-modal growth region, the secondary instability stage, the intermittent spot region and the fully developed turbulent boundary-layer region. The y-coordinate is scaled with δ^* which is the displacement thickness for a laminar boundary layer based on the length from the leading edge. Near the leading edge, the boundary layer is very close to the Blasius form, whereas further downstrean it starts to deviate, such that an increased velocity is observed in the inner half of the boundary layer and a decrease in the outer half. Figure 2(*b*) shows this behaviour for five positions in the range $700\,\mathrm{mm} < x < 1100\,\mathrm{mm}$, where the amplitude of the deviation is scaled with its maximum value. The deviation is seen to collapse nicely for the different x-positions, showing a nearly self-similar development (see also Talamelli, Westin & Alfredsson 2000). The increase close to the wall means an increased skin friction as compared with the Blasius boundary layer.

The distribution of u_{rms}, for small x shows a maximum approximately in the middle of the laminar boundary layer (figure 2*c*). However, as the flow becomes turbulent, the maximum shifts towards the wall, becomes more peaky, whereafter further downstream its amplitude starts to decrease. In figure 2(*d*) the maximum value of u_{rms}^2 is shown as a function of the Reynolds number based on x, and it is clearly shown that, during the initial phase, the growth in u_{rms}^2 is linear with x. Thereafter, it increases faster, reaches a maximum and then saturates. Also plotted in this figure is the position of the maximum in the u_{rms}-distribution, it is constant at

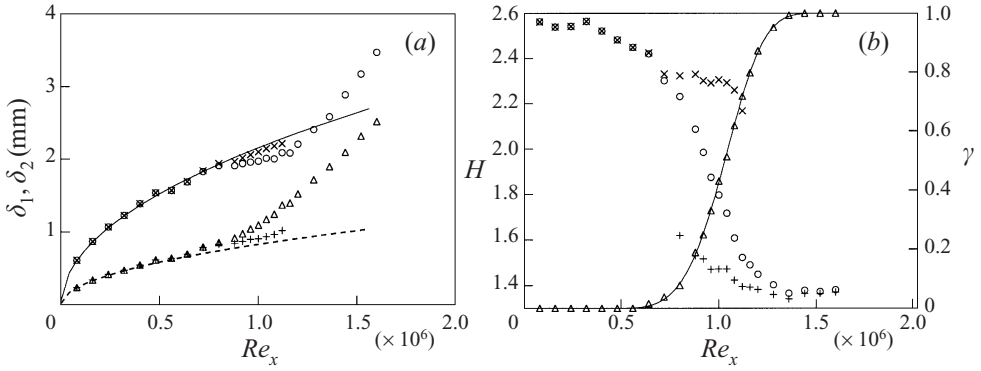

FIGURE 3. Measurements of (*a*) ○, δ_1; △, δ_2, and ×, δ_1; +, δ_2 calculated under periods of laminar flow. (*b*) ○, shape factor (H_{12}) for full signal; ×, H_{12} measured during laminar periods; +, H_{12} measured during turbulent periods; △, intermittency factor γ. Same data as in figure 2.

$y/\delta^* = 1.3$ during the linear growth region, but further downstream it becomes closer to the wall. For a turbulent boundary layer, one would expect the maximum of u_{rms} to be located at $y^+ \approx 15$, and an estimate of this position is given in figure 2(*d*).

Figure 3 shows the development of some integral parameters of the boundary layer. In figure 3(*a*) the measured displacement (δ_1) and momentum-loss (δ_2) thicknesses are shown, together with lines showing the theoretical development for a Blasius boundary layer. In the transitional region, δ_1 decreases slightly whereas δ_2 increases above the Blasius curve. The latter is related to the fact that the average skin friction increases owing to the occurrence of turbulent spots. This region, i.e. the region in between the Blasius-like and the turbulent regions, is usually called the intermittent region, in the sense that turbulent spots occur intermittently and grow as they travel downstream. This region can therefore be viewed as being composed of laminar-like and turbulent-like periods with some kind of blending period in between.

In an analysis of this type of transitional flows, discrimination between turbulent and laminar flow is valuable, not only to estimate the intermittency function, but also to obtain separated statistics of the measured data into laminar and turbulent cases. Several methods for the discrimination have been proposed which use some criterion function with a threshold to determine the flow status. One difficulty is that the threshold value directly affects the result of the intermittency estimate. Kuan & Wang (1990) developed a general method to determine the threshold, the so-called dual-slope method, which was further developed by Matsubara, Alfredsson & Westin (1998). The latter approach gave a value of γ that was fairly independent of the y-position inside the boundary layer at which the measurements were made.

With a method to distinguish laminar and turbulent periods of the signal it is possible to obtain a better understanding of the transitional region. In figure 3(*b*), the distribution of γ is shown, which has the expected behaviour of zero value for small Re_x and approaches 1 for high values. The shape factor $H = \delta_1/\delta_2$ starts at around 2.6 and decreases to a value of 1.4 in the turbulent region, a value which is consistent with that to be expected for turbulent boundary layers at this Reynolds number. Also plotted in both figures 3(*a*) and 3(*b*) are the values obtained when sorting the signal into laminar and turbulent parts. In the laminar part, the shape factor decreases slightly with increasing Re_x. Figure 2(*b*) shows that in this region there is an increase in mean velocity near the wall and a decrease further out. The effect on the displacement thickness is small, but leads to an increase in δ_2 which

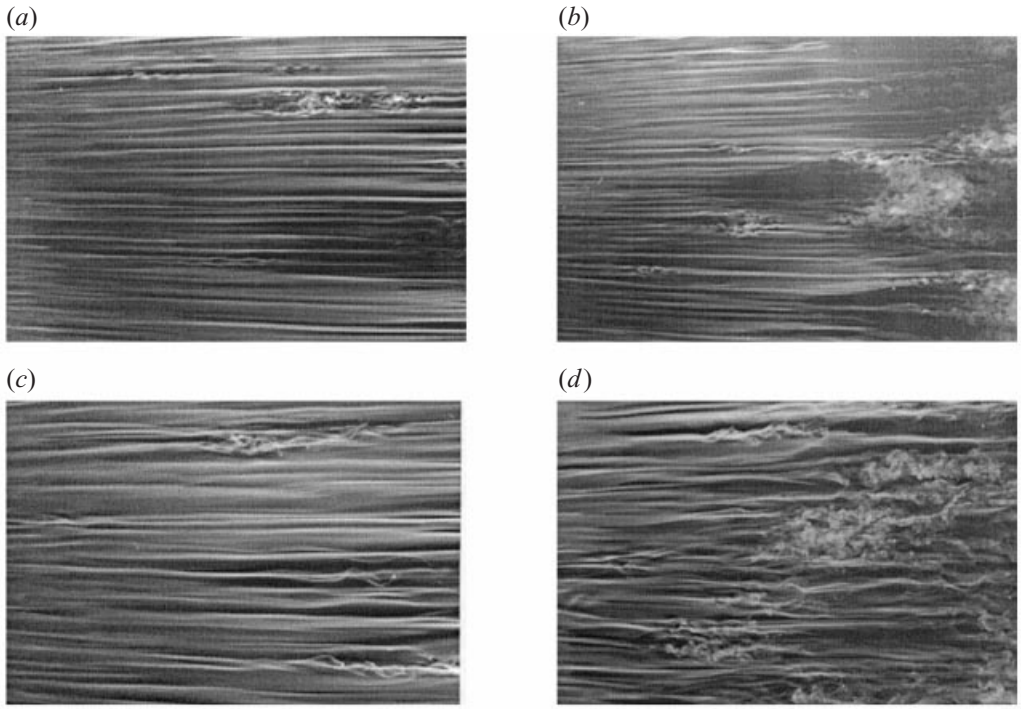

FIGURE 4. Flow visualization of streaky structures in boundary layers affected by FST. The flow direction is from left to right. The streamwise extent of pictures is $220\,\mathrm{mm} < x < 700\,\mathrm{mm}$. The smoke slot is positioned at $x = 175\,\mathrm{mm}$. (*a*) Grid A, $U_\infty = 6\,\mathrm{m\,s^{-1}}$; (*b*) grid A, $U_\infty = 8\,\mathrm{m\,s^{-1}}$; (*c*) grid E, $U_\infty = 2\,\mathrm{m\,s^{-1}}$; (*d*) grid E, $U_\infty = 3\,\mathrm{m\,s^{-1}}$.

lowers the shape factor. The change in H_{12} is a direct consequence of the nonlinear interaction between the streaky structures and the mean flow. In the turbulent region, the formation and propagation of turbulent spots contribute to the skin friction, and, therefore, an increase in δ_2.

4. Measurements of disturbance structure

In this section we will analyse the experimental results obtained both from flow visualization and two-probe hot-wire measurements in terms of the structure of the transitional boundary layer.

4.1. *Flow-visualization data*

Figure 4 shows flow-visualization results for grids B and E, having 1.5% and 6.6% turbulence level at the plate leading edge, respectively. All photographs show an area for which $220\,\mathrm{mm} < x < 700\,\mathrm{mm}$ and $-150\,\mathrm{mm} < z < 150\,\mathrm{mm}$. For the low-turbulence case, the free-stream velocities in the two photographs are 6 and $8\,\mathrm{m\,s^{-1}}$, respectively (the corresponding Reynolds-number ranges based on x for the two cases are $0.9\text{–}2.8 \times 10^5$ and $1.2\text{–}3.7 \times 10^5$, respectively). The streaky structure of the smoke layer is apparent in both cases and the streaks have a spanwise scale of around 1 cm, although the scale seems somewhat smaller at the higher velocity. For both cases, some streaks are seen to develop a streamwise waviness of relatively short wavelength. These wiggles usually develop into turbulent spots, and in the upper half

of figure 4(*a*) an incipient spot can be distinguished. At the downstream end of figure 4(*b*) around $z = 0$ mm, a fully developed turbulent spot can be seen. The turbulent region of the spot is shown as a diffuse light region and it has the characteristic downstream-pointing V-shape. Behind the spot there is a lack of smoke, owing to the fact that when the spot passed over the smoke layer the smoke was mixed into the spot and then convected with the spot.

For the high-turbulence case shown in figures 4(*c*) and 4(*d*) the velocities are 2 and 3 m s^{-1}, respectively (the corresponding Reynolds-number ranges based on x for the two cases are 0.3–0.9×10^5 and 0.44–1.4×10^5, respectively). Also here streaky structures are observed, although the spanwise scale is larger in this case. This is, to some extent, due to the fact that the turbulence scales generated by grid E at these velocities are larger, but may also depend on the fact that the boundary layer is thicker owing to the lower free-stream velocities. Also here a wavy type of motion may be observed on the streaks before they break down to turbulence; however, turbulent spots cannot be distinguished easily in this case.

In figure 5, a typical sequence showing the development of a streak instability is shown. The time between frames is 20 ms. The free-stream velocity is 2 m s^{-1} and the speed of the structure was estimated to $0.5\,U_\infty$. It can be seen that the streak first becomes wavy, the wave amplitude increases and that suddenly there is a break up of the streaky structure, which is observed through dispersion of the smoke.

The streamwise lengthscale of the streaky structure increases in the downstream direction. This becomes evident by analysing video recordings choosing one line of the CCD camera at three different x-positions and plotting this line as function of time. In figure 6 the resulting pictures are shown for $x = 360, 720$ and 1000 mm. The spanwise size is approximately 300 mm and the time period is 5 s. The data are obtained using grid E at $U_\infty = 1.2$ m s^{-1}. The size of the streamwise scale is seen to increase with the downstream position. At $x = 1000$ mm some streaks can be identified for about half the recorded time. For the most upstream x-position the scales seem rather short, however, it should be borne in mind that the flow-visualization pictures using smoke show an integrated picture of the development of the smoke layer, and the time available to redistribute the smoke increases in the downstream direction.

The spanwise scale of the streaks can be estimated from figures such as these, both by direct observation, and also by determining the spanwise correlation of the light intensity. Figure 7 shows such correlation measurements for data obtained with grid A. The correlation function has the expected variation with Δz, showing a zero crossing around 5 mm and then a minimum (this position will be denoted by Δz_{min}, closely corresponding to half the streak spacing) whereafter it approaches zero.

In figure 8, we show the value Δz_{min} for two different grids at various velocities. The correlation functions were determined at 8 downstream positions in each case. It is shown in figure 8(*a*) that the variation in physical units is not so large along the plate, for some cases it decreases and for others it increases. However, by scaling Δz_{min} with the displacement thickness (calculated based on the distance from the leading edge) it is interesting to note that all data seem to approach a value of approximately $3\delta^*$ at the most downstream position. This value corresponds approximately to the boundary-layer thickness of a Blasius boundary-layer.

4.2. *Hot-wire data*

In the following, we will discuss measurements of the streamwise velocity with one or two probes. Figure 9 shows time signals and spectra obtained at five y-positions, where the largest y is in the free-stream and the others are distributed throughout

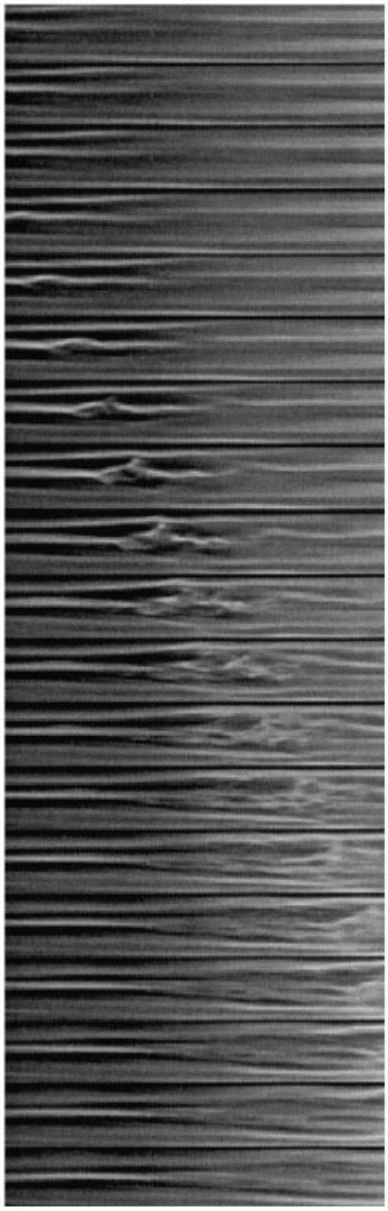

FIGURE 5. Sequence of streak breakdown with 20 ms between pictures. Grid E. $U_\infty = 2\,\mathrm{m\,s^{-1}}$. $400\,\mathrm{mm} < x < 600\,\mathrm{mm}$.

the boundary layer. As can be seen the character of the signal changes dramatically as the plate is approached. This can also be clearly seen in the spectra (figure 9*b*) where the low-frequency content is seen to increase and the high-frequency content to decrease as compared to the free stream. As shown in figure 2(*c*) the maximum in u_{rms} corresponds roughly to $y/\delta^* = 1.3$ and it is clear from the spectra that a large contribution to the energy in this region is from the low frequencies.

In figure 10 two-point spanwise correlations are shown for all three grids (A, B and E) at three different downstream positions, $x = 50$, 200 and 600 mm. The

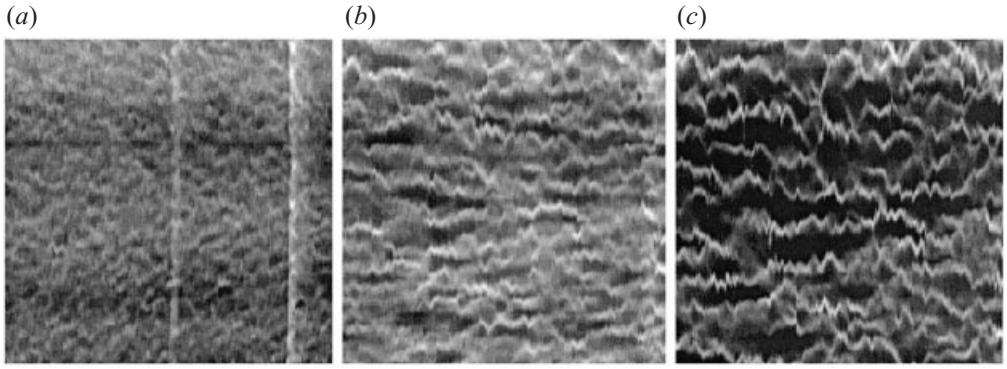

FIGURE 6. Records over time (horizontal scale corresponds to 5 s) at three different x-positions obtained from video signal. Width (vertical scale) of picture is approximately 300 mm. Grid E. $U_\infty = 1.2\,\mathrm{m\,s^{-1}}$. (*a*) $x = 360$ mm; (*b*) $x = 720$ mm; (*c*) $x = 1000$ mm.

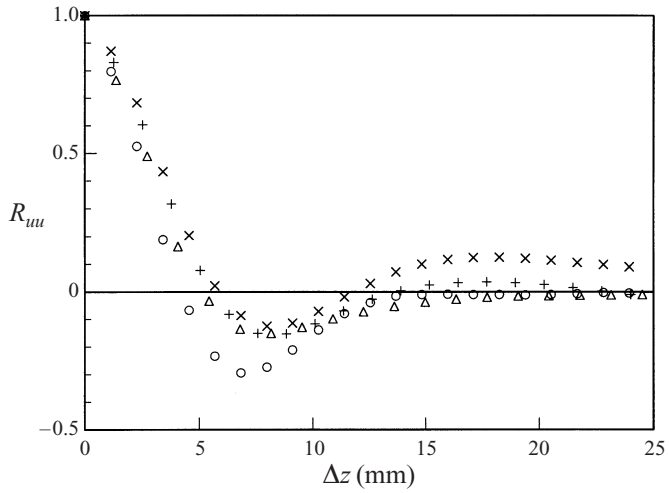

FIGURE 7. Correlation function of brightness in spanwise direction obtained from records like those in figure 6. Grid A. ×, $x = 720$ mm, $U_\infty = 6.0\,\mathrm{m\,s^{-1}}$; +, $x = 1000$ mm, $U_\infty = 6.0\,\mathrm{m\,s^{-1}}$; ○, $x = 500$ mm, $U_\infty = 8.0\,\mathrm{m\,s^{-1}}$; △, $x = 1000$ mm, $U_\infty = 8.0\,\mathrm{m\,s^{-1}}$.

measurements with grids A and B are at $U_\infty = 6.0\,\mathrm{m\,s^{-1}}$ whereas $U_\infty = 3.0\,\mathrm{m\,s^{-1}}$ for grid E. Figure 10(*a*) shows the correlations in the free stream where the spanwise separation distance has been normalized with the grid mesh width. As can be seen, the data for grids A and E collapse fairly well, however, grid B shows a slight shift at short separations. As was noted previously, all grids have a Taylor microscale for the transverse velocity component of approximately 5 mm at $U_\infty = 8\,\mathrm{m\,s^{-1}}$, and since the mesh width is smaller for grid B than for grid A the shift in figure 10(*a*) is consistent with a constant Taylor microscale. However, the smaller free-stream velocity for grid E in this case leads to a larger Taylor microscale, which may explain the collapse of the correlations between grids A and E.

Figures 10(*b*) to 10(*d*) show measurements for the different grids made at the position of maximum u_{rms}, but also in the free stream for comparison. The boundary-layer thickness is approximately 3.5 times larger at $x = 600$ mm as compared to $x = 50$ mm, but as can be seen the correlation function for small separations (<5 mm)

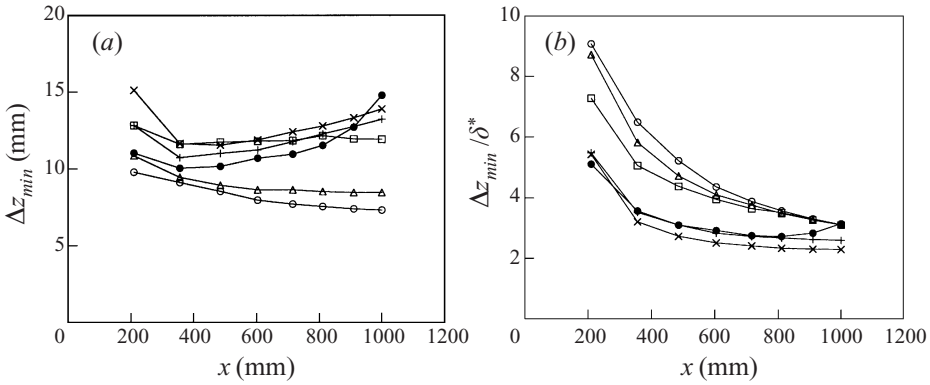

FIGURE 8. The spanwise distance to the first minimum (Δz_{min}) in the two-point correlation as function of downstream distance for two different grids obtained from correlation functions such as those in figure 7. Grid B: □, $U_\infty = 3.0\,\mathrm{m\,s^{-1}}$; △, $U_\infty = 6.0\,\mathrm{m\,s^{-1}}$; ○, $U_\infty = 8.0\,\mathrm{m\,s^{-1}}$. Grid E: ×, $U_\infty = 1.2\,\mathrm{m\,s^{-1}}$; +, $U_\infty = 1.7\,\mathrm{m\,s^{-1}}$; ●, $U_\infty = 2.0\,\mathrm{m\,s^{-1}}$. (*a*) Data in physical measure; (*b*) scaled with the local boundary-layer displacement thickness.

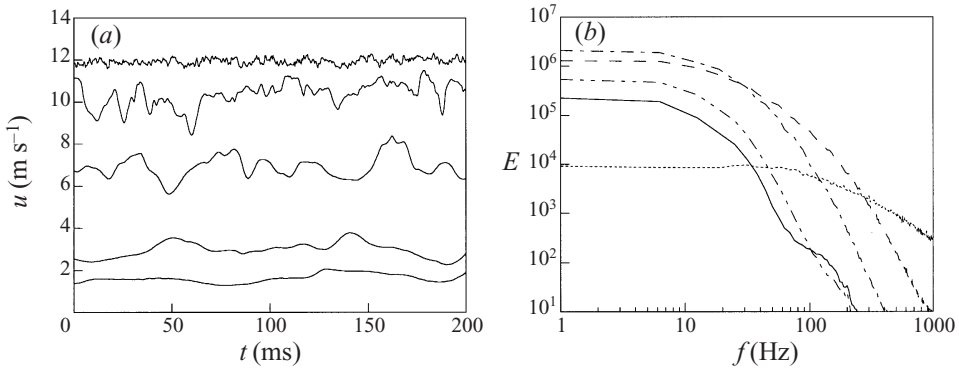

FIGURE 9. Hot-wire measurements at $U_\infty = 12\,\mathrm{m\,s^{-1}}$ and $x = 500\,\mathrm{mm}$. (*a*) Time signals from 4 different heights inside the boundary layer and one in the free stream; (*b*) the corresponding spectra ···, $y/\delta^* = 17.8$; — — —, $y/\delta^* = 1.78$; — · —, $y/\delta^* = 1.05$; — · · —, $y/\delta^* = 0.43$; ——, $y/\delta^* = 0.25$. In (*a*) the same heights are shown and are distinguished through their mean velocity.

is independent of x. Inside the boundary layer, the correlation function has a clear minimum for the two most downstream positions. These minima can be used to estimate the spanwise scale of the disturbance. In figure 11, the distance to this minimum normalized with the local displacement thickness is plotted as a function of the Reynolds number for three different grids. The spanwise size of the disturbance initially differs between the grids but seems to asymptotically approach a value close to $3\delta^*$. These results are in accordance with those obtained from the flow visualization in figure 8(*b*) and will be further discussed in § 5.

Another way to illustrate the structure inside the boundary layer is through spanwise correlation measurements at various values of y and showing the results in terms of a contour plot for the correlation function. This is done in figure 12 ($U_\infty = 5.0\,\mathrm{m\,s^{-1}}$, $x = 1600\,\mathrm{mm}$) where it is clearly shown how a region of negative correlation appears in the boundary layer. The boundary-layer thickness is here approximately 11 mm and the region of negative correlation is confined inside the boundary layer. This region has an aspect ratio of about 1 and the minimum value is around −0.35. The

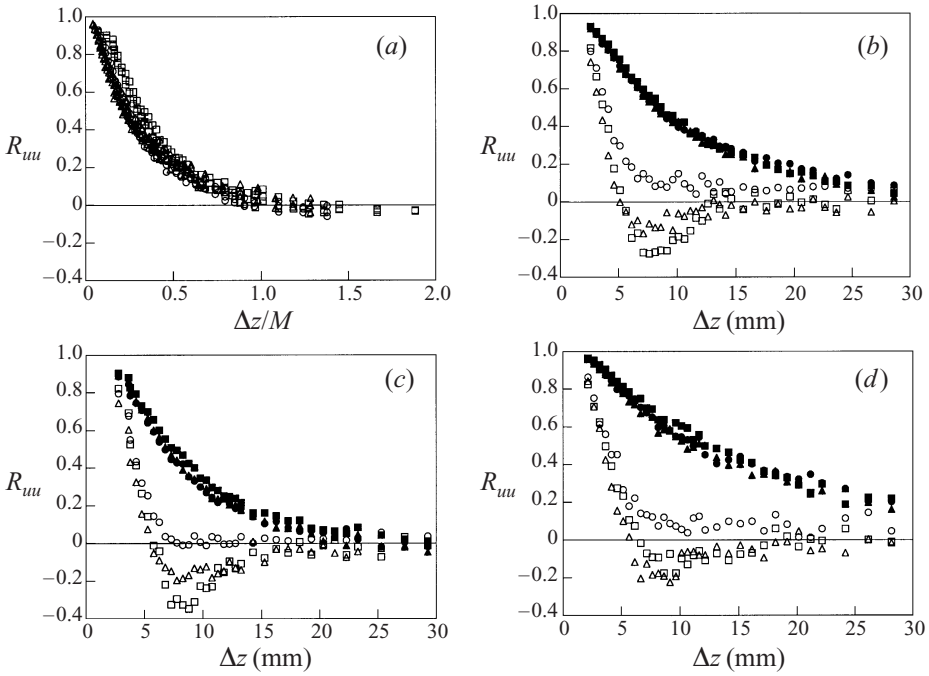

FIGURE 10. Spanwise correlation obtained from two hot-wire probes. (*a*) Measurements in the free stream with three different grids: ○, grid A; □, grid B; Δ, grid E, spanwise separation normalized with the grid mesh width. For each grid, measurements are made at $x = 50$, 200 and 600 mm. (*b*)–(*d*) Measurements in the free stream (filled symbols) and at $y/\delta^* = 1.2$ (unfilled symbols). ○, $x = 50$ mm; Δ, $x = 200$ mm; □, $x = 600$ mm. (*b*) Grid A, $U_\infty = 6.0\,\mathrm{m\,s^{-1}}$. (*c*) Grid B, $U_\infty = 6.0\,\mathrm{m\,s^{-1}}$. (*d*) Grid E, $U_\infty = 3.0\,\mathrm{m\,s^{-1}}$.

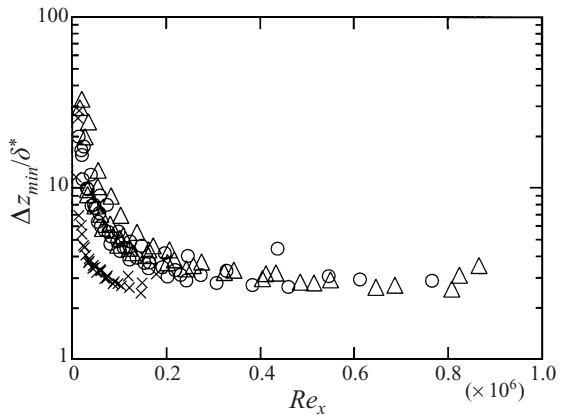

FIGURE 11. Spanwise distance to first minimum obtained from correlations such as those in figure 10. ○, grid A; △, grid B; ×, grid E.

figure clearly support the view that the dominating structure in the boundary layer consists of high- and low-speed regions, with an average separation of 2δ ($\approx 6\delta_*$).

Figure 13 shows both (*a*) streamwise, and (*b*) spanwise wavenumber spectra of the streamwise velocity measured at $y/\delta^* = 1.2$. The spanwise spectral results are based on simultaneous velocity measurements at two spanwise positions and obtained by taking the Fourier transform of each time signal. From these transformed signals

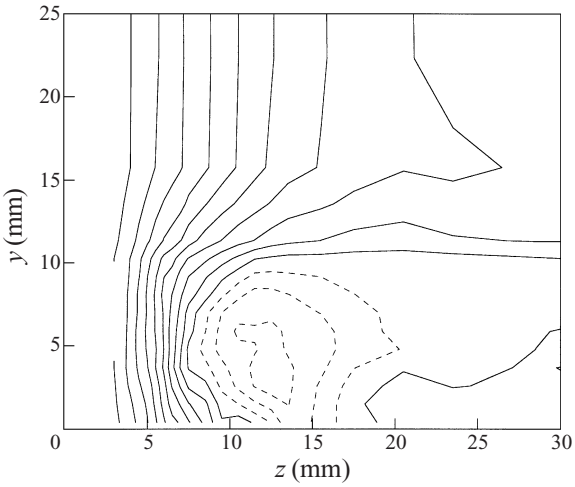

FIGURE 12. Contour map of spanwise correlation in (y,z)-plane with grid B. $x = 1600\,\mathrm{mm}$, $U_\infty = 5.0\,\mathrm{m\,s^{-1}}$. Contour spacing is 0.1 and negative contours are dashed. Number of points in $y = 15$, in $z = 26$.

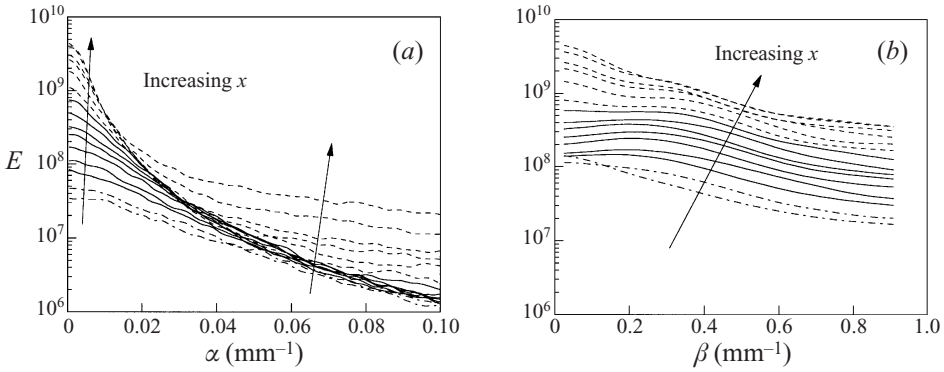

FIGURE 13. Typical spectra for different downstream positions. Grid A. $U_\infty = 5.0\,\mathrm{m\,s^{-1}}$. (*a*) Streamwise wavenumber spectra, obtained from frequency spectra, $\alpha = 2\pi f/U_\infty$; (*b*) spanwise wavenumber spectra. For both (*a*) and (*b*), spectra are obtained at 15 different x-positions, the spectra can be distinguished by the trend that increasing x shifts the spectra upwards. $-\cdot-$, $x = 50,\ 80$; ——, $x = 120, 150, 200, 250, 300, 400, 500$; $-\,-\,-$, 600, 800, 1000, 1200, 1600, 2000 mm.

the spanwise correlation for each of the frequency components can be calculated by multiplication of the complex Fourier coefficients. To obtain the power spectra, the Fourier transform of the spanwise correlations finally has to be taken. The streamwise spectra (obtained from the frequency spectra) in figure 13(*a*) show that for small x the low wavenumber region increases, whereafter the energy growth also occurs for high wavenumbers. This is consistent with the view that longitudinal streaks increase in amplitude (growth at low wavenumbers), whereafter they break down to turbulence (growth at high wavenumbers). In the spanwise spectra (figure 13*b*), the amplitude decreases slightly with β and the overall amplitude increases with x as expected.

It is possible to further illustrate the downstream development of the disturbance energy by an appropriate scaling of the spectra shown in figure 13. For the spanwise spectra the energy is scaled with Re_x, i.e. if the energy is growing linearly with x as assumed for non-modal growth, the spectra should collapse. Figure 14(*b*) does

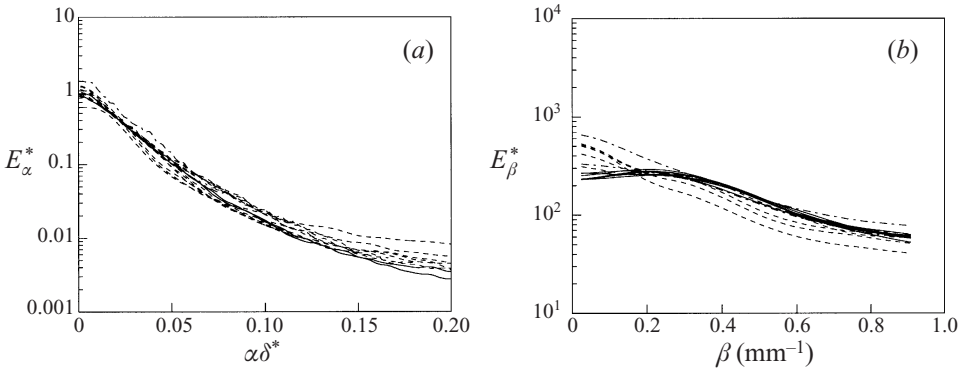

FIGURE 14. Non-dimensionalized wavenumber spectra of figure 13, (*a*) streamwise wavenumber spectra, wavenumber scaled with local displacement thickness according to Blasius solution, and energy scaled with Re_x; (*b*) spanwise wavenumber spectra, energy scaled with Re_x.

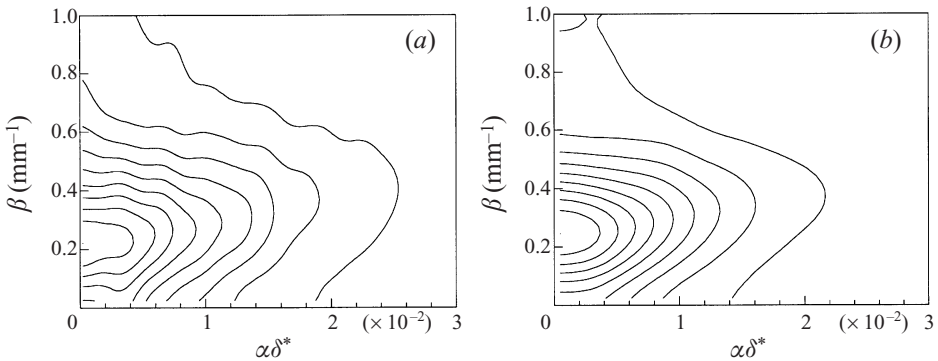

FIGURE 15. Two dimensional wavenumber spectra. Grid B. $U_\infty = 5.0\,\mathrm{m\,s^{-1}}$. (*a*) $x = 200\,\mathrm{mm}$; (*b*) $x = 800\,\mathrm{mm}$. Contour spacing is 10% of maximum value.

indeed show such a collapse, except for the x-positions furthest downstream. Note also that the spanwise coordinate is still dimensional. It was found that this gave the best collapse of the data. This may be compared with the results obtained from the correlation measurements in figure 8 where it was found that the position of minimum correlation was almost constant in physical size for each grid. On the other hand, figure 14(*a*) shows a remarkable collapse if the streamwise wavenumber is scaled with δ^* and the energy scaled similarly. All spectra in the low wavenumber region are found to collapse giving a strong indication for non-modal growth of streamwise oriented structures. The finding that the streamwise wavenumber scales with δ^*, i.e. $x^{1/2}$ was unexpected, but was found also for the other grids used.

Another way to illustrate the disturbance structure in the boundary layer is to construct two-dimensional wavenumber spectra. The results of such an evaluation are displayed in figure 15 where the spectra at two x-positions are shown, $x = 200\,\mathrm{mm}$ and $x = 800\,\mathrm{mm}$. The spanwise wavenumber is dimensional at both x-positions. The streamwise wavenumber, on the other hand, is scaled with δ^*, whereas the amplitudes of the spectra are normalized with their maximum values. The clear similarity of the two spectra is evident, and the maximum energy peak located at $\alpha = 0$ again indicates the dominance of streamwise oriented structures.

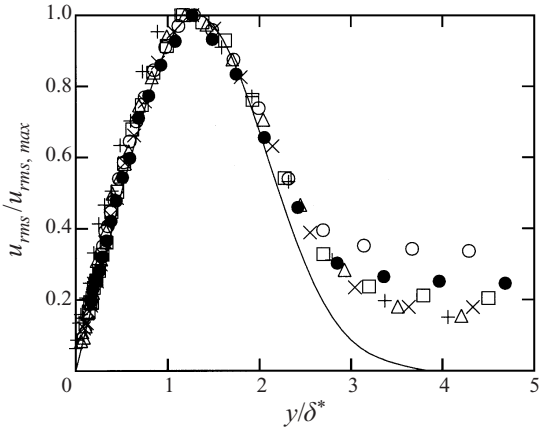

FIGURE 16. Comparison to the optimal disturbance growth theory (Luchini 2000). u_{rms}-profiles, ○, $x = 200$ mm; ●, $x = 300$ mm; □, $x = 400$ mm; ×, $x = 500$ mm; △, $x = 600$ mm; +, $x = 700$ mm; ——, theory.

5. Discussion and summary

The present work is an extensive study of the influence of free-stream turbulence on the disturbance development in laminar boundary layers and the subsequent breakdown to turbulence. The data presented in this article is a concentrate of several years of experiments, but chosen to show the significant features of the disturbance structure and its growth. The interpretations of the initial stages of the disturbance behaviour are strongly influenced by recent work on non-modal (transient) growth in shear flows. The breakdown of the streaky structures seems to be associated with secondary instability which develops owing to the influence of high and low-speed fluid regions.

We have presented results both from smoke flow visualization and two-point hot-wire measurements. It is, at first, not obvious how the smoke field is correlated to the velocity field. Recent results obtained by simultaneous PIV-measurements and smoke visualization (Alfredsson & Matsubara 2000) clearly indicate that the smoke-filled streaky regions correspond to regions of lower velocity than the mean. Correspondingly, the smoke-free regions represent high streamwise velocity.

The measurements of the streamwise velocity disturbance (u_{rms}, see figure 2c, d) show how the initial growth is proportional to $x^{1/2}$. This is in accordance with Luchini (2000). Also, the disturbance distribution is in accordance with this theory, see figure 16. Here, several profiles of u_{rms} obtained at various x-positions are normalized with their respective maximum and, as can be seen, these profiles are self-similar over most of the boundary layer. At the outer edge of the boundary layer, the experiments do not tend to zero since the free-stream turbulence is still present, whereas in the theory, the disturbance outside the boundary layer is zero. It should be pointed out that both the growth and disturbance profiles obtained with other theoretical approaches, such as those of Andersson *et al.* (1999) and Goldstein & Wundrow (1998) give similar results.

An important issue is the spanwise scale of the streaky structure which we have investigated through correlation measurements using both hot-wire and flow-visualization data. On the one hand, both flow visualization and hot-wire measurements in the present work show that there is no dramatic change in the spanwise scale (in physical units) with downstream distance. On the other hand, it seems that the scale approaches the boundary-layer thickness (see figures 8b and 11). This may

be due to an initially strong mismatch between the scales in the free-stream turbulence and the optimal disturbance in the boundary layer, but as the boundary layer grows, there is a better match between the initial scale and the optimal disturbance size. In the theoretical work by Luchini (2000) and Andersson *et al.* (1999), it was found that the optimal scale was approximately 1.4δ. In these studies, only the linear development of the disturbance is studied and it is clear that, in the region where the spanwise size of the disturbance in our case approaches the boundary-layer thickness, the amplitude is fairly high and the disturbance can no longer be viewed as linear.

The contour map of the correlation function (figure 12) shows that the dominant structures inside the boundary layer consist of regions of high- and low-speed fluid. It also shows that the height of the structure is close to the boundary-layer thickness and that its cross-flow aspect ratio is approximately 1 far from the leading edge.

The flow visualizations show that the length of the streamwise structures increase in the downstream direction (see e.g. figure 6). This is also seen from hot-wire spectra using the Taylor hypothesis. From the spectral data, it was seen that the streamwise length of the structures are proportional to δ^* or $x^{1/2}$. This was an unexpected new finding and there is so far no theoretical explanation for this result. The spanwise spectra, on the other hand, seem to be fairly independent of the downstream distance (figure 14*b*), if the wavenumber is plotted in physical units. Similar results are obtained from the two-point correlations (see figure 10). The spectra also show an astonishing similarity when scaled as in figure 14. Similar results were also obtained for various free-stream velocities if the energy was scaled with the free-stream velocity squared. For transition prediction methods, these scalings may be a valuable finding if it is possible to find a relation between the disturbance energy and the breakdown.

This work was supported by the Swedish Research Council for Engineering Sciences (TFR) and the Göran Gustafsson foundation. M. M. was partly supported by a JSPS Research Fellowship for Young Scientists. The spanwise correlation mesurements using two hot wires were made in cooperation with Dr Andrey Bakchinov.

REFERENCES

Alfredsson, P. H. & Matsubara, M. 2000 Free-stream turbulence, streaky structures and transition in boundary layer flows. *AIAA Paper* 2000-2534.

Andersson, P., Berggren, M. & Henningson, D. S. 1999 Optimal disturbances and bypass transition in boundary layers. *Phys. Fluids* **11**, 134–150.

Arnal, D. & Juillen, J. C. 1978 Contribution experimentale à l'étude de la receptivité d'une couche limite laminaire, à la turbulence de l'ecoulement general. *ONERA Rap. Tech.* 1/5018 AYD.

Bakchinov, A. A., Westin, K. J. A., Kozlov, V. V. & Alfredsson, P. H. 1998 Experiments on localized disturbances in a flat plate boundary layer. Part 2. Interaction between localized disturbances and TS-waves. *Eur. J. Mech.* B/*Fluids* **17**, 847–873.

Bertolotti, F. P. 1997 Response of the Blasius boundary layer to free stream vorticity. *Phys. Fluids* **9**, 2286–2299.

Boiko, A. V., Westin, K. J. A., Klingmann, B. G. B., Kozlov, V. V. & Alfredsson, P. H. 1994 Experiments in a boundary layer subjected to free stream turbulence. Part 2. The role of TS-waves in the transition process. *J Fluid Mech.* **281**, 219–245.

Butler, K. M. & Farrell, B. F. 1992 Three-dimensional optimal perturbations in viscous shear flow. *Phys. Fluids* A **4**, 1637–1650.

Dryden, H. L. 1937 Air flow in the boundary layer near a plate. *NACA Tech. Rep.* 562.

Ellingsen, T. & Palm, E. 1975 Stability of linear flow. *Phys. Fluids* **18**, 487–488.

Elofsson, P. A. & Alfredsson, P. H. 1998 An experimental study of oblique transition in plane Poiseuille flow. *J. Fluid Mech.* **358**, 177–202.

Elofsson, P. A., Kawakami, M. & Alfredsson, P. H. 1999 Experiments on the stability of streamwise streaks in plane Poiseuille flow. *Phys. Fluids* **11**, 915–930.

Goldstein, M. E. & Wundrow, D. W. 1998 On the environmental realizability of algebraically growing disturbances and their relation to Klebanoff modes. *Theoret. Comput. Fluid Dyn.* **10**, 171–186.

Grek, H. R., Kozlov, V. V. & Ramazanov, M. P. 1990 Receptivity and stability of the boundary layer at a high turbulence level. In *Laminar-Turbulent Transition* (ed. D. Arnal & R. Michel), pp. 511–521. Springer.

Gustavsson, L. H. 1991 Energy growth of three-dimensional disturbances in plane Poiseuille flow. *J. Fluid Mech.* **224**, 241–260.

Kendall, J. M. 1985 Experimental study of disturbances produced in a pre-transitional laminar boundary layer by weak free stream turbulence. *AIAA Paper* 85-1695.

Kendall, J. M. 1998 Experiments on boundary-layer receptivity to freestream turbulence. *AIAA Paper* 98-0530.

Klebanoff, P. S. 1971 Effects of free-stream turbulence on a laminar boundary layer. *Bull. Am. Phys. Soc.* **16**.

Kosorygin, V. S. & Polyakov, N. P. 1990 Laminar boundary layers in turbulent flows. In *Laminar-Turbulent Transition* (ed. D. Arnal & R. Michel), pp. 573–578. Springer.

Kuan, C. L. & Wang, T. 1990 Investigation the intermittent behavior of transitional boundary layer using a conditional averaging technique. *Exp. Thermal Fluid Sci.* **3**, 157–173.

Landahl, M. T. 1980 A note on an algebraic instability of inviscid parallel shear flows. *J. Fluid Mech.* **98**, 243–251.

Leib, S. J., Wundrow, D. W. & Goldstein, M. E. 1999 Effect of free-stream turbulence and other vortical disturbances on a laminar boundary layer. *J. Fluid Mech.* **380**, 169–203.

Luchini, P. 1996 Reynolds-number-independent instability of the boundary layer over a flat surface. *J. Fluid Mech.* **327**, 101–115.

Luchini, P. 2000 Reynolds number independent instability of the boundary-layer over a flat surface: optimal perturbations. *J. Fluid Mech.* **404**, 289–309.

Matsubara, M., Alfredsson, P. H. & Westin, K. J. A. 1998 Boundary layer transition at high levels of free stream turbulence. Paper 98-GT-248 ASME. International Gas Turbine and Aeroengine Congr. and Exhibition, Stockholm, 2–5 June, 1998.

Reddy, S. C., Schmid, P. J., Baggett, J. S. & Henningson, D. S. 1998 On stability of streamwise streaks and transition thresholds in plane channel flows. *J. Fluid Mech.* **365**, 269–303.

Roach, P. E. & Brierly, D. H. 1992 The influence of a turbulent free stream on zero pressure gradient transitional boundary layer development. Part I: Test cases T3A and T3B. In *Numerical Simulation of Unsteady Flows and Transition to Turbulence*, pp. 319–347. Cambridge University Press.

Schmid, P. J. & Henningson, D. S. 1992 A new mechanism for rapid transition involving a pair of oblique waves. *Phys. Fluids* A **4**, 1986–1989.

Suder, K. L., O'Brien, J. E. & Reshotko, E. 1988 Experimental study of bypass transition in a boundary layer. *NASA Tech. Mem.* 100913.

Talamelli, A., Westin, K. J. A. & Alfredsson, P. H. 2000 An experimental investigation of the response of hot-wire X-probes in shear flows. *Exps Fluids* **28**, 425–435.

Taylor, G. I. 1939 Some recent developments in the study of turbulence. In *Proc. 5th Intl Congr. Appl. Mech.* pp. 294–310, Wiley.

Westin, K. J. A. 1997 Laminar–turbulent boundary layer transition influenced by free stream turbulence. PhD thesis, TRITA-MEK 1997:10, Department of Mechanics, KTH.

Westin, K. J. A., Bakchinov, A. A., Kozlov, V. V. & Alfredsson, P. H. 1998 Experiments on localized disturbances in a flat plate boundary layer. Part 1. The receptivity and evolution of a localized free stream disturbance. *Eur. J. Mech.* B/*Fluids* **17**, 823–846.

Westin, K. J. A., Boiko, A. V., Klingmann, B. G. B., Kozlov, V. V. & Alfredsson, P. H. 1994 Experiments in a boundary layer subjected to free stream turbulence. Part 1. Boundary layer structure and receptivity. *J. Fluid Mech.* **281**, 193–218.

Westin, K. J. A. & Henkes, R. A. W. M. 1997 Application of turbulence models to by-pass transition. *J. Fluids Engng* **119**, 859–866.

Waleffe, F. 1997 On a self-sustaining process in shear flows. *Phys. Fluids* A **9**, 883–900.